



TECHNICAL REPORT AMR-SS-08-12

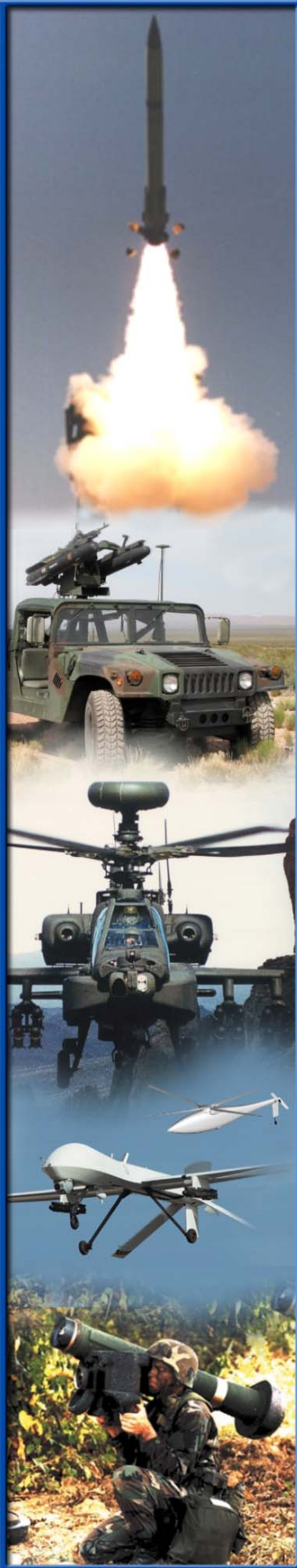
ERROR ESTIMATION FOR THREE TURBULENCE MODELS: INCOMPRESSIBLE FLOW

Milton E. Vaughn, Jr.

System Simulation and Development Directorate
Aviation and Missile Research, Development, and
Engineering Center

January 2008

Approved for public release: distribution is unlimited.



DESTRUCTION NOTICE

FOR CLASSIFIED DOCUMENTS, FOLLOW THE PROCEDURES IN DoD 5200.22-M, INDUSTRIAL SECURITY MANUAL, SECTION II-19 OR DoD 5200.1-R, INFORMATION SECURITY PROGRAM REGULATION, CHAPTER IX. FOR UNCLASSIFIED, LIMITED DOCUMENTS, DESTROY BY ANY METHOD THAT WILL PREVENT DISCLOSURE OF CONTENTS OR RECONSTRUCTION OF THE DOCUMENT.

DISCLAIMER

THE FINDINGS IN THIS REPORT ARE NOT TO BE CONSTRUED AS AN OFFICIAL DEPARTMENT OF THE ARMY POSITION UNLESS SO DESIGNATED BY OTHER AUTHORIZED DOCUMENTS.

TRADE NAMES

USE OF TRADE NAMES OR MANUFACTURERS IN THIS REPORT DOES NOT CONSTITUTE AN OFFICIAL ENDORSEMENT OR APPROVAL OF THE USE OF SUCH COMMERCIAL HARDWARE OR SOFTWARE.

REPORT DOCUMENTATION PAGE			Form Approved OMB No. 074-0188
Public reporting burden for this collection of information is estimated to average 1 hour per response, including the time for reviewing instructions, searching existing data sources, gathering and maintaining the data needed, and completing and reviewing this collection of information. Send comments regarding this burden estimate or any other aspect of this collection of information, including suggestions for reducing this burden to Washington Headquarters Services, Directorate for Information Operations and Reports, 1215 Jefferson Davis Highway, Suite 1204, Arlington, VA 22202-4302, and to the Office of Management and Budget, Paperwork Reduction Project (0704-0188), Washington, DC 20503			
1. AGENCY USE ONLY	2. REPORT DATE January 2008	3. REPORT TYPE AND DATES COVERED Final	
4. TITLE AND SUBTITLE Error Estimation for Three Turbulence Models: Incompressible Flow			5. FUNDING NUMBERS
6. AUTHOR(S) Milton E. Vaughn, Jr.			
7. PERFORMING ORGANIZATION NAME(S) AND ADDRESS(ES) Commander, U.S. Army Research, Development, and Engineering Command ATTN: AMSRD-AMR-SS-AT Redstone Arsenal, AL 35898			8. PERFORMING ORGANIZATION REPORT NUMBER TR-AMR-SS-08-12
9. SPONSORING / MONITORING AGENCY NAME(S) AND ADDRESS(ES)			10. SPONSORING / MONITORING AGENCY REPORT NUMBER
11. SUPPLEMENTARY NOTES			
12a. DISTRIBUTION / AVAILABILITY STATEMENT Approved for public release: distribution is unlimited.			12b. DISTRIBUTION CODE A
13. ABSTRACT (Maximum 200 Words) In order to facilitate the application of Computational Fluid Dynamics (CFD) tools by aerodynamic designers, an assessment of error was made for the Menter Shear Stress Transport (SST), Spalart-Allmaras, and Nichols-Nelson Hybrid (RANS/LES) SST turbulence models. The assessment was made for incompressible flow over a smooth flat plate of unit length. Correlations of the error in drag coefficient with initial grid point spacing, expressed in terms of y^+ , were discovered for each model. It was found that the correlations were nonlinear and could be expressed in terms of the sine function.			
14. SUBJECT TERMS Applied Computational Fluid Dynamics (CFD), Aerodynamic Design, Error, Error Estimation, Turbulence Model, Menter Shear Stress Transport, Spalart-Allmaras, Nichols-Nelson, Hybrid Turbulence Model, RANS/LES			15. NUMBER OF PAGES 32
			16. PRICE CODE
17. SECURITY CLASSIFICATION OF REPORT UNCLASSIFIED	18. SECURITY CLASSIFICATION OF THIS PAGE UNCLASSIFIED	19. SECURITY CLASSIFICATION OF ABSTRACT UNCLASSIFIED	20. LIMITATION OF ABSTRACT SAR

NSN 7540-01-280-5500

Standard Form 298 (Rev. 2-89)
Prescribed by ANSI Std. Z39-18
298-102

TABLE OF CONTENTS

	<u>Page</u>
I. INTRODUCTION	1
II. METHODOLOGY	1
III. RESULTS AND DISCUSSION	8
A. The Menter SST and Spalart-Allmaras RANS Models	8
B. The Nichols-Nelson Hybrid (RANS/LES) SST Model.....	13
IV. SUMMARY.....	18
REFERENCES	19

LIST OF ILLUSTRATIONS

<u>Figure</u>	<u>Title</u>	<u>Page</u>
1.	Computational Domain for Numerical Experiments	2
2.	Typical Grid for Numerical Experiments	3
3.	Profiles of u^+ for the Menter SST Turbulence model at $x/L=0.9308$ — Refined Grids	8
4.	Profiles of u^+ for the Spalart-Allmaras Turbulence Model at $x/L=0.9308$ —Refined Grids	9
5.	Local Skin Fiction Coefficient, $c_f(x)$, for the Menter SST Turbulence Model—Refined Grids	10
6.	Local Skin Fiction Coefficient, $c_f(x)$, for the Spalart-Allmaras Turbulence Model—Refined Grids.....	11
7.	Error Versus Initial Point Spacing for the Menter SST Turbulence Model	12
8.	Error Versus Initial Point Spacing for the Spalart-Allmaras Model	12
9.	Contours of L_T/L_G for $y^+ = 3$ —Guideline Grid.....	14
10.	Contours of L_T/L_G for $y^+ = 3$ —Highly Refined Grid	14
11.	Profiles of u^+ for the Nichols-Nelson Hybrid SST Turbulence Model at $x/L=0.9308$ —Guideline Grids.....	16
12.	Local Skin Fiction Coefficient, $c_f(x)$, for the Nichols-Nelson Hybrid SST Model—Guideline Grids.....	17
13.	Error Versus Initial Point Spacing for Nichols-Nelson Hybrid SST Model	18

LIST OF TABLES

<u>Table</u>	<u>Title</u>	<u>Page</u>
1.	Computational Setup for Numerical Experiments.....	2
2.	Initial Cell Sizes Correlated with y^+ for $x = 1 L$	5
3.	Time Steps Used for Nichols-Nelson Computations.....	6
4.	Comparison of Drag Coefficients from the Menter SST, Spalart-Allmaras, and Nichols-Nelson Hybrid (RANS/LES) SST Turbulence Models for $L_T/L_G < 2$ Throughout Most of the Flowfield—RANS Results Reported for the Most Refined Grids	15

I. INTRODUCTION

The discipline of Computational Fluid Dynamics (CFD) has progressed to the point that Navier-Stokes flow solvers can be used to support the aerodynamic design process in a practical manner [1 through 7]. However, a significant impediment exists in that there are currently no general, quantitative guidelines available to assist aerodynamic designers in constructing suitable computational grids. To speak to this need, an initial effort was made by Vaughn [8] to develop “rules of thumb” for incompressible, laminar, flat plate flows. It proved to be successful. Yet, turbulent flows must be addressed for any such rules to have general usefulness.

As a first step in doing so, it is necessary to ascertain the relationship between the error produced by a selected turbulence model—for a parameter of interest—and cell spacing. Since the practical application of CFD is often focused on producing adequate force and moment coefficients for the configuration of interest, it was decided to explore the behavior of turbulence model error with respect to total drag on a flat plate. To minimize the number of physical complexities involved, the study was conducted for a smooth plate within a uniform, incompressible flowfield with no pressure gradient.

There are numerous turbulence models available for use. However, the Menter Shear Stress Transport (SST) [9] and Spalart-Allmaras [10] models have the distinction of widespread use among Reynolds-Averaged Navier-Stokes (RANS) solvers for steady-state flows. In addition, the hybrid RANS/LES (Large Eddy Simulation) model developed by Nichols and Nelson [11] has shown itself to be comparable to the Spalart Detached Eddy Simulation (DES) technique [12] for flows with significant unsteady motion. And it has been shown to be superior to DES for unsteady cavity and shear layer flows [11]. Because of their extensive utility, these three methods were selected for examination in this study.

II. METHODOLOGY

The inquiry started with the grid construction guidelines developed for incompressible, laminar, flat plate flow in Reference 8. Hence, the one-sided hyperbolic tangent distribution function was applied at the leading edge to distribute points in all coordinate directions. With this foundation, the computational domain shown in Figure 1 and summarized in Table 1 was created for a flat plate of one foot length with $L = 1$. Doing this kept the plate entirely within the Region of Interest shown in the figure. A typical grid created in this manner is shown in Figure 2. Wind-US 1.0 was chosen as the flow solver because it embodies widely-used solution methods such that the results would have meaning for the general CFD community [8, 13].

The large plate from NACA TN 4017 [14] was selected for the examination. It had a freestream velocity of 58 feet-per-second with a Reynolds number of 3.23×10^5 at the station $x = 11.17$ inches ($0.9308 L$) where velocity profiles were measured. However, since the drag was not measured, it was calculated at $x = 1 L$ (1 foot) where the Reynolds number was 3.47×10^5 .

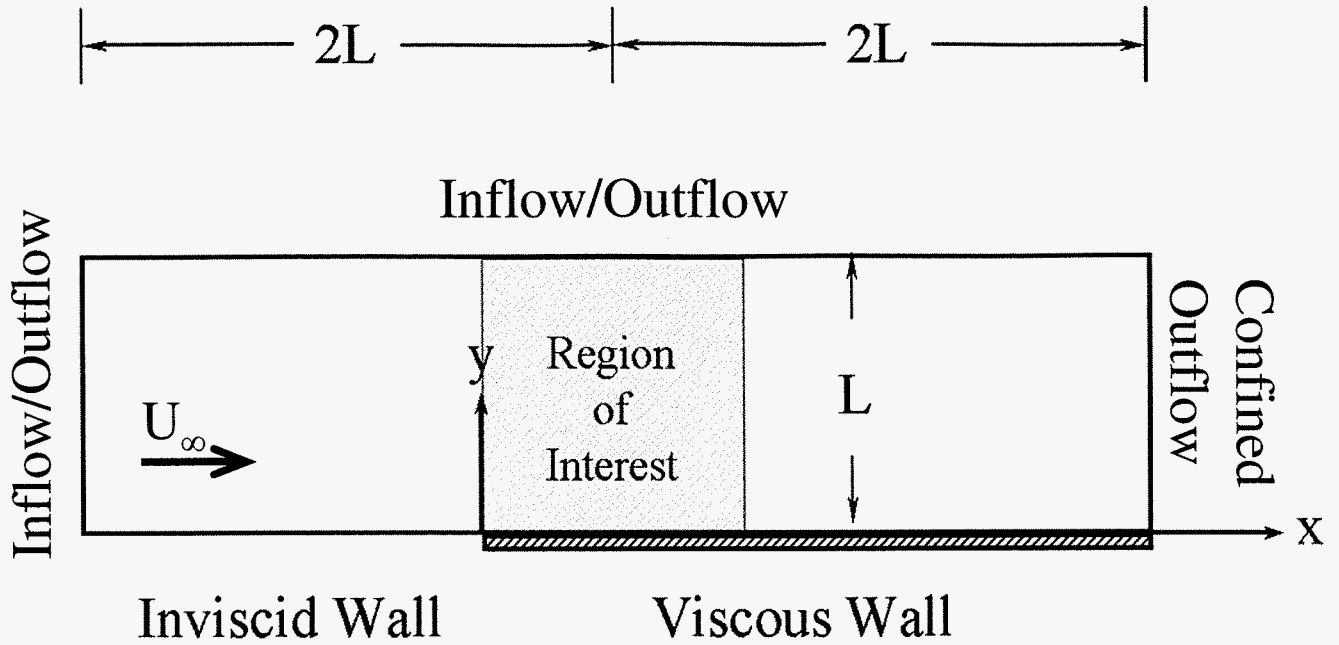


Figure 1. Computational Domain for Numerical Experiments

Table 1. Computational Setup for Numerical Experiments

Quantity	Value
Algorithm	Scalar Implicit
CFL Number	1.3
TVD Setting	On
Boundary Condition–Upstream	Inflow/Outflow
Boundary Condition–Upper	Inflow/Outflow
Boundary Condition–Downstream	Confined Outflow
Grid Structure	10 Vertical Slices
Number of CPUs for Parallel Computations	10
Boundary Location with respect to Region of Interest–Upstream	2L
Boundary Location with respect to Region of Interest–Upper	1L
Boundary Location with respect to Region of Interest–Downstream	2L

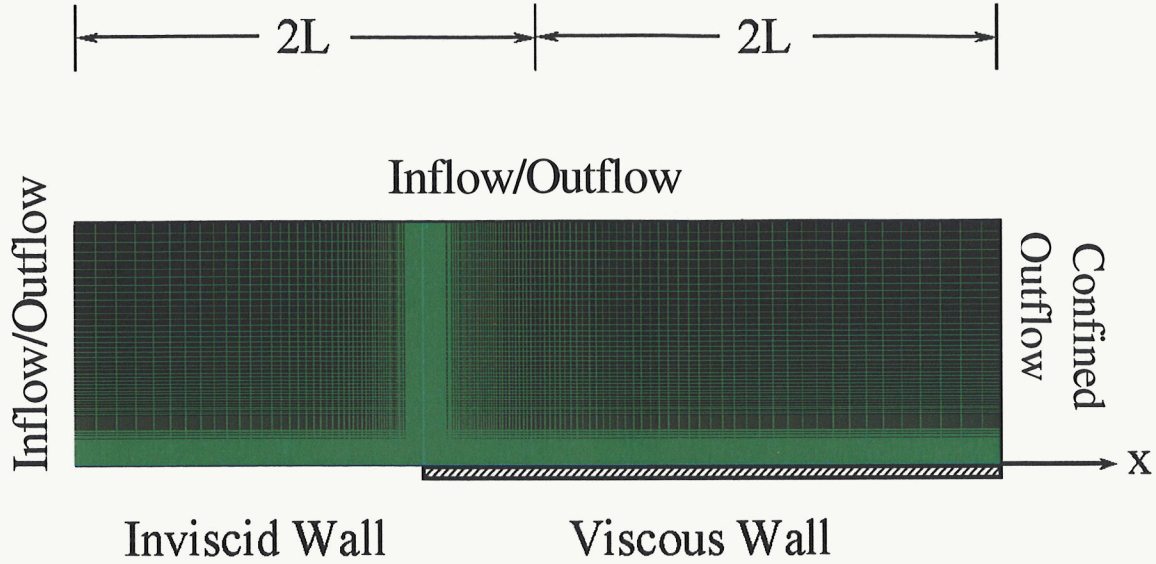


Figure 2. Typical Grid for Numerical Experiments

It was recognized that when gridding to the wall it is common practice to place points within the laminar sublayer, that is, where $y^+ \leq 5$. However, it was also considered to be useful to demonstrate the necessity of doing so and the consequence of failing to do so. Thus, it was decided to compute solutions with initial points both within and outside the laminar sublayer, specifically at $y^+ = 1, 2, 3, 4, 5, 7, 9$ and 15 .

The computations were considered to be routine for the two RANS models. However, with respect to the Nichols-Nelson model, it was recognized that, "... this new class of turbulence models is inherently grid-size dependent because increasing the grid resolution allows smaller and smaller turbulent scales to be resolved" [15]. Further, it was also acknowledged that, "... all of the [hybrid] models will tend to the RANS limit if the grid spacing becomes too coarse to support the turbulent scales of the flow" [15]. In addition, Nichols recommended that the ratio of turbulent length scale to grid length scale be at least two in order to achieve reasonably grid-independent solutions for the unsteady cases he studied.

This ratio is given by L_T/L_G where [11, 13]

$$L_T = \max \left(6.0 \sqrt{\frac{v_{tRANS}}{\Omega}}, \frac{k_{RANS}^{3/2}}{\epsilon_{RANS}} \right) \quad (1)$$

$$L_G = \max(\Delta x, \Delta y, \Delta z) \quad (2)$$

$\nu_{t_{RANS}}$, k_{RANS} , ϵ_{RANS} are the respective kinematic viscosity, turbulent kinetic energy, and dissipation rate of the RANS turbulence model; and $\Delta x, \Delta y, \Delta z$ are the local Cartesian grid lengths in physical space. It was hoped that Nichols's recommendation would also work in reverse such that by decreasing L_T/L_G to less than two an adequate, steady-state RANS solution could be obtained. If this turned out to be true, then the hybrid turbulence model could also be applied to steady-state flows. Although the Nichols-Nelson Hybrid model can use any two-equation turbulence method for its RANS component, the Menter SST technique has been found to work well in flows with severe adverse pressure gradients and separation [9]. Hence, this form of the Nichols-Nelson approach was selected for use in the study.

To facilitate sizing the grid cells along the plate, a direct relationship was sought between y , y^+ and readily available flow parameters. This process started with the definition of the y^+ non-dimensional normal coordinate given by [16]

$$y^+ = \frac{y v_*}{\nu} \quad (3)$$

where v_* is von Karman's frictional velocity [16] defined by

$$v_* = \sqrt{\frac{\tau_w}{\rho}} \quad (4)$$

Then White's formula for skin friction on a flat plate in turbulent flow [17] was called upon to find the shear stress at the wall, τ_w . This was done by manipulating the definition of skin friction coefficient, $c_f(x) = \tau_w / (0.5 \rho_\infty U_\infty^2)$, within Equation 4 to obtain

$$v_* = \sqrt{\frac{1}{\rho_\infty} \left[\frac{1}{2} \rho_\infty U_\infty^2 \frac{0.455}{\ln^2(0.06 \text{Re}_x)} \right]} \quad (5)$$

This expression for the frictional velocity was inserted in to Equation 3 and simplified to the forms

$$y^+ = \frac{0.477 y \text{Re}_x}{x \ln(0.06 \text{Re}_x)} \quad (6)$$

and

$$y = \frac{y^+ x \ln(0.06 \text{Re}_x)}{0.477 \text{Re}_x} \quad (7)$$

Equation 7 was exercised afterwards to calculate the physical size of the cells along the plate, that is, the initial point spacing, for the desired values of y^+ at the point of interest. The values produced for $x = 1 L$ are listed in Table 2. To reiterate, these initial cell sizes were exercised with the one-sided hyperbolic tangent distribution function and the previously mentioned guidelines to create the first computational domains. However, grid refinement studies were also conducted both normal to and along the plate using the same sized cells adjacent to the surface. Tables listing the numbers of cells comprising each grid are provided in chapter 4 of Reference 13. It should be noted that the same solution domains were used to evaluate all three turbulence models.

Table 2. Initial Cell Sizes Correlated with y^+ for $x = 1 L$

y^+	Initial Cell Size
1	$6.12 \times 10^{-5} L$
2	$1.20 \times 10^{-4} L$
3	$1.80 \times 10^{-4} L$
4	$2.40 \times 10^{-4} L$
5	$3.01 \times 10^{-4} L$
7	$4.21 \times 10^{-4} L$
15	$9.02 \times 10^{-4} L$

It should also be stated that other relations and curve fits for skin friction were found in Reference 16. However, White's formula is founded on Spalding's "Law of the Wall" [17] which relies upon the "inner variables" y^+ and $u^+ = u/v_*$, where u is the streamwise velocity component. It was thereby presumed to be as exact as is currently possible. Additionally, it is recommended as a very accurate relation for turbulent flat plates [17]. Because of these points and the fact that it has a somewhat simpler form than the other relations and curve fits, White's skin friction equation was selected for use in deriving Equations 6 and 7.

The CFL number was kept at the default value of 1.3 for Wind-US when employing the Spalart-Allmaras and SST turbulence models. However, this parameter permits the value of the time step to vary in each cell depending on its dimensions. Since the SST version of the Nichols-Nelson Hybrid model requires a constant physical time step for each cell, those calculations were instead performed in the time-accurate mode. Accordingly, the CFL number was replaced with the TIMESTEP parameter. To enable the signal propagation in the smallest cells to be commensurate with that of the RANS runs—as opposed to being too slow—a relationship was empirically developed to relate the desired CFL number and the minimum cell spacing ($\Delta s_{\text{minimum}}$) to the global timestep. This formula was determined to be

$$\Delta t = 8.397 \times 10^{-4} \frac{\text{sec}}{\text{ft}} CFL \Delta s_{\text{minimum}} \quad (8)$$

and it produced the timestep values shown in Table 3.

Table. 3. Time Steps Used for Nichols-Nelson Computations

	Initial Cell Size $\Delta s_{\text{minimum}}$	Δt (seconds)
1	$6.12 \times 10^{-5} L$	6.681×10^{-8} used 1.0×10^{-7}
2	$1.20 \times 10^{-4} L$	1.310×10^{-7}
3	$1.80 \times 10^{-4} L$	1.965×10^{-7}
4	$2.40 \times 10^{-4} L$	2.620×10^{-7}
5	$3.01 \times 10^{-4} L$	3.254×10^{-7}
7	$4.21 \times 10^{-4} L$	4.552×10^{-7}
15	$9.02 \times 10^{-4} L$	5.979×10^{-7}

White's formula for drag on a flat plate in turbulent flow [17] was used as the point of reference for total drag comparisons. It was developed by integration of his skin friction formula and was therefore considered to be quite accurate [17]. As with the skin friction equation, it was selected over other formulas and curve fits found in Reference 16 because of its somewhat simpler form and stated correctness [17]. The formula is written as

$$C_D = \frac{0.523}{\ln^2(0.06 \text{Re}_x)} \quad (9)$$

and was used in conjunction with

$$E_{\text{White}} = \frac{C_{D_{\text{computed}}} - C_{D_{\text{White}}}}{C_{D_{\text{White}}}} \quad (10)$$

to compute the error in drag coefficient. Note that E_{White} is the error with respect to the White's value, $C_{D_{\text{computed}}}$ is the drag coefficient of the computed solution, and $C_{D_{\text{White}}}$ is White's value of drag coefficient. In addition, Guo's recently developed Self-Similarity Law [18]—which encompasses Coles's law of the Wall [19]—provided a means of evaluating the computed velocity profiles.

The very first RANS computations for $y^+ = 1, 3$ and 5 were executed for 72,000 cycles to assure convergence. In addition, a duplicate calculation with the SST model for $y^+ = 1$ was performed for 36,000 cycles to check for convergence at an earlier iteration number. A computation was also made with the block implicit algorithm to test for algorithm differences. It was found that the solution was fully converged by 36,000 cycles, and that the scalar implicit algorithm provided the same results as the block implicit method, but in less time. All the hybrid solutions were iterated for 72,000 cycles.

After the flowfield calculations were completed, the Grid Convergence index (GCI) of Roache [20] was determined for the solutions sets of each turbulence model. This was done to quantify the numerical error present in each computation. It is based on values from a fine grid and a coarser one, denoted by subscripts c and f , and it is given by

$$GCI_{f,c} = \frac{3}{r^p - 1} |\varepsilon| \quad (11)$$

where $\varepsilon = (f_c - f_f)/f_f$, $r = h_c/h_f$ (the cell size ratio between a coarse and a fine grid), p is the order of the solution algorithm, f_c = the value of the quantity of interest for the coarse grid, and f_f = the value of the quantity of interest for the fine grid. Wind-US had previously been shown to be second-order accurate using the Method of Manufactured solutions [21], so p was set to 2. The values of h_c and h_f were taken from Table 2. In addition, Roache's formula for testing computed results to determine if they reside within the asymptotic region was invoked as well. This equation, given by [20]

$$GCI_{2,3} = r^p GCI_{1,2} \quad (12)$$

is said to be approximately satisfied when solution values for three computations—denoted via the subscripts 1, 2 and 3—approach the exact value in a monotonic fashion. It was applied to results for $y^+ = 1, 2, 4$ and 7 since r is a nearly constant value for these successive y^+ pairings.

The findings of the “GCI” effort were that: (1) GCI = 2 percent for the Menter SST and Spalart-Allmaras RANS models, and (2) the RANS solutions for $1 \leq y^+ \leq 4$ do reside within the asymptotic region. Thus, the numerical error of the RANS computations was quantified at 2 percent. The GCI was also found for the Nichols-Nelson Hybrid approach. However, it is important to recall that the same components of a computational model must be operating during each calculation for the GCI to be valid. This was not the case with the Nichols-Nelson Hybrid method. As previously mentioned, this technique resolves smaller turbulence scales with each refined grid. Consequently, its RANS component is only active for grid cells too large to capture the turbulence. When the computational grid is sufficiently refined to capture a significant portion of the turbulent field, the RANS component becomes inactive for a large part of the computation. Therefore, it was not clear how to use the grid refinement studies to quantify the numerical error in these particular calculations. Nonetheless, since the SST model constituted the RANS constituent of the hybrid approach, and since the drag values were seen to be very similar to the Menter SST results for $y^+ > 1$, it was presumed that the numerical error would be very similar at 2 percent.

III. RESULTS AND DISCUSSION

A. The Menter SST and Spalart-Allmaras RANS Models

Profiles of the non-dimensional streamwise velocity, $u^+ = u/v_*$, are presented for the Menter SST and Spalart-Allmaras RANS turbulence models in Figures 3 and 4. It can be seen that as y^+ decreases from 15 to 1, the profiles for both methods approach those for $y^+ = 1$ and 2 in a monotonic fashion. In fact, the profiles for $y^+ = 1$ and 2 overlay each other, thereby establishing grid independence. It can also be seen that the profiles closely follow Guo’s Self-Similarity Law from the wall up to $y^+ = 10$, but that above that point deviations occur that become more pronounced as the freestream flow is approached.

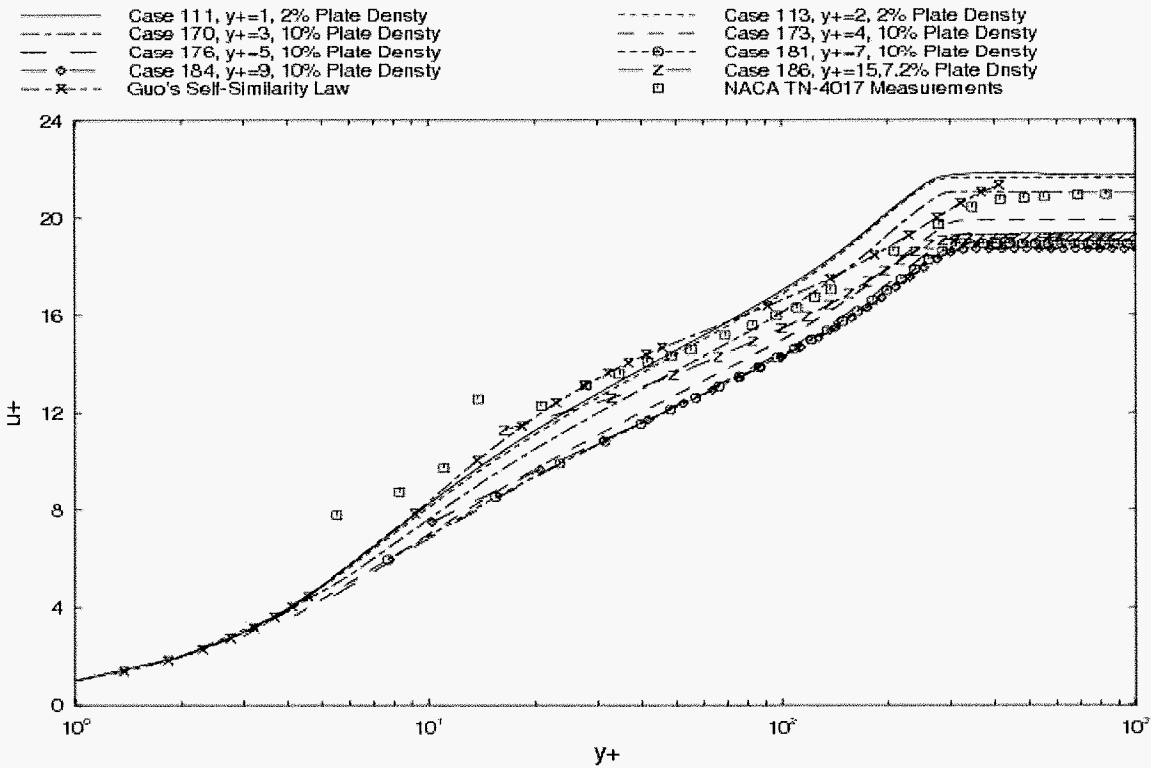


Figure 3. Profiles of u^+ for the Menter SST Turbulence model at $x/L=0.9308$ —Refined Grids

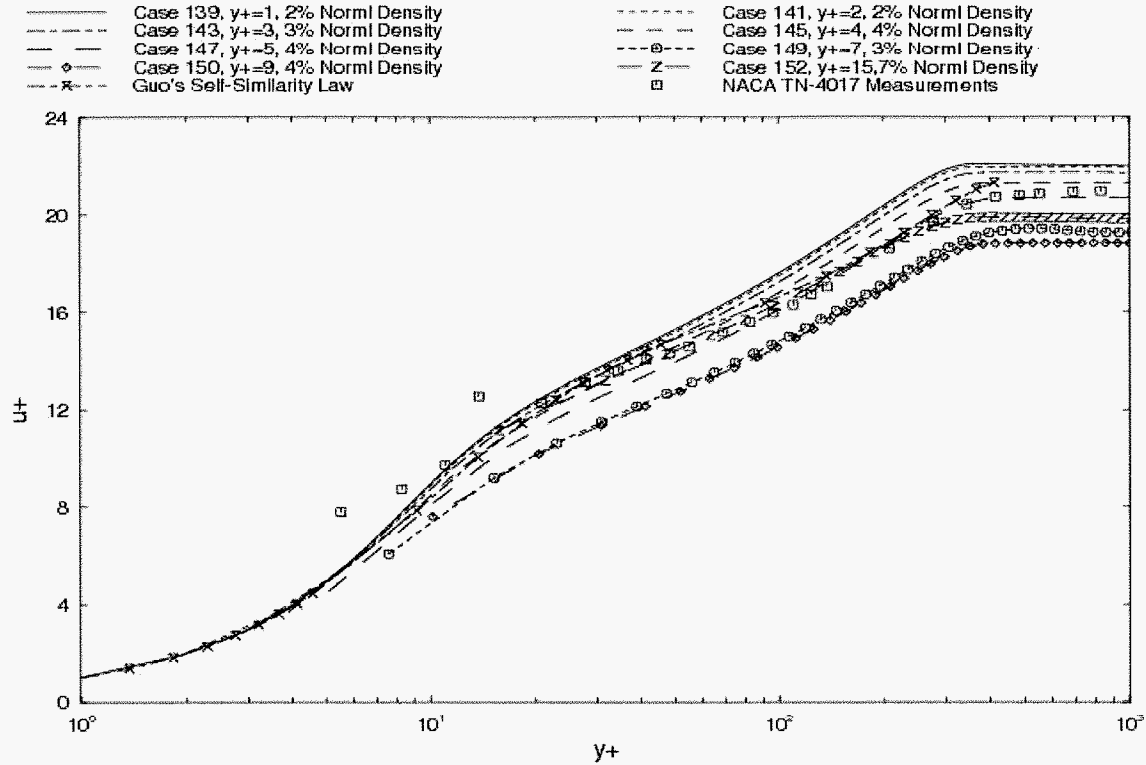


Figure 4. Profiles of u^+ for the Spalart-Allmaras Turbulence Model at $x/L=0.9308$ —Refined Grids

The reason for this may be that Guo’s equation was developed from pipe flow data, but it was adapted and applied to the flat plate. Such an alteration is sound since according to Schlichting [16] “the velocity profiles in the boundary layer on a plate and inside a pipe are identical, if the maximum velocity U and the radius R of the circular tube are replaced by the free-stream velocity U_∞ and the boundary-layer thickness δ of the plate.” However, Guo adjusted his wake correction for the outer portion of the boundary layer based on axisymmetric flow. Consequently, it is reasonable for the plate computations to agree with his curve near the wall and to increasingly differ from it when moving towards the freestream.

In addition, it can be perceived that the measured velocities from NACA TN-4017 differ noticeably from the trends of Guo’s curve as well as those for $y^+ = 1$ and 2—even when disregarding the apparently bad data point above $y^+ = 10$. Furthermore, the deviation becomes increasingly large towards the wall. This behavior suggests that the measured flow was not yet fully turbulent—a reasonable expectation since the boundary layer was not tripped in the experiment.

The corresponding skin friction plots are shown in Figures 5 and 6. In these graphs, it can be discerned that: (1) these curves also vary with y^+ , (2) the skin friction lines approach those of $y^+ = 1$ and 2 as y^+ decreases, and (3) the lines for $y^+ = 1$ and 2 overlay each other. These points are more readily observed by examining the downstream portions of the curves where the plotting symbols are less dense. However, it can easily be detected in Figure 5 that all the Menter SST graphs exhibit the artificial transition from laminar to turbulent flow that is characteristic of all two-equation turbulence models [22]. This skin friction “bucket” occurs with all such predictions, but was particularly prevalent for the low-Reynolds number cases herein because they exist at the very low end of the turbulent flow regime. In contrast to this behavior, Figure 6 shows that the Spalart-Allmaras model does not produce such a feature.

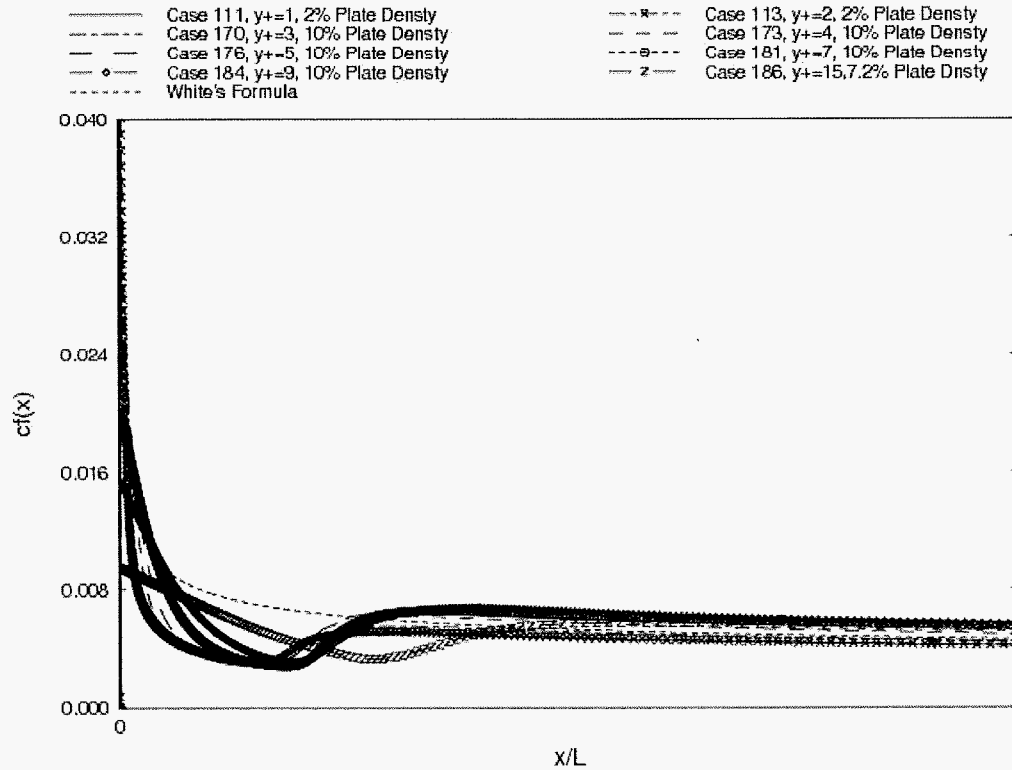


Figure 5. Local Skin Fiction Coefficient, $c_f(x)$, for the Menter SST Turbulence Model—Refined Grids

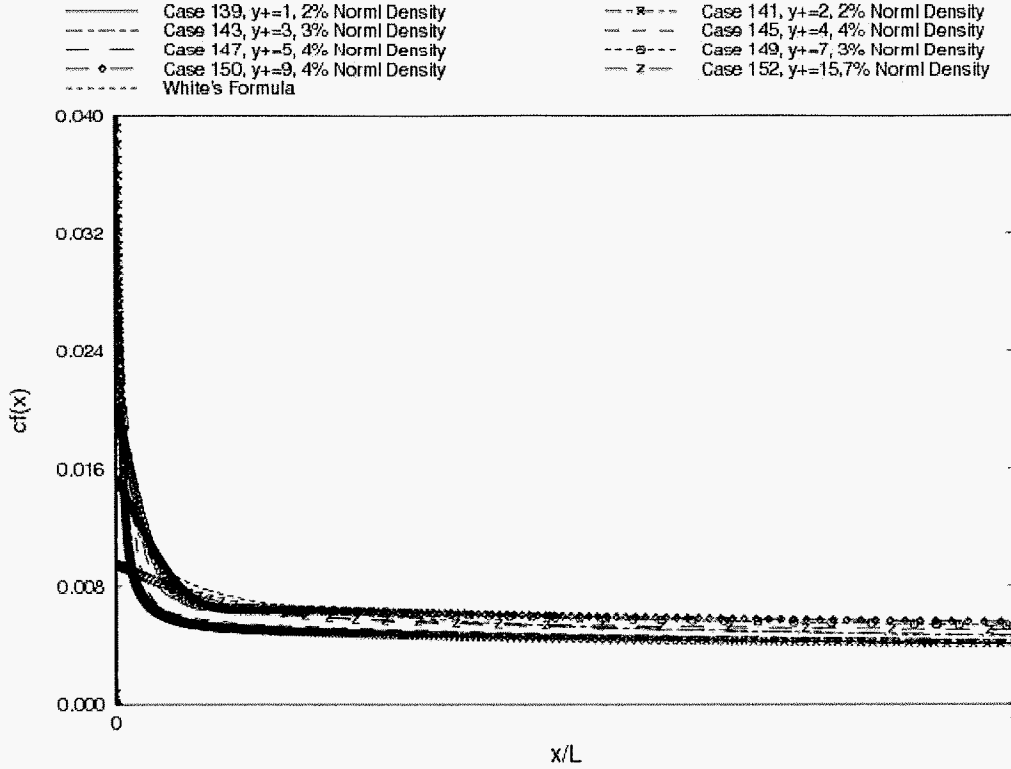


Figure 6. Local Skin Friction Coefficient, $c_f(x)$, for the Spalart-Allmaras Turbulence Model—Refined Grids

Results for the error in drag coefficient of both RANS models are exhibited in Figures 7 and 8. It can clearly be seen that both techniques produce negative as well as positive error—a feature that was simply due to the computed drag coefficient being less than White’s value of 5.3×10^{-3} . It was not expected that White’s formula would provide an absolute standard of reference. Rather, it served as the best available point of comparison. So the presence of negative error was not surprising. What seemed more striking, though, were the nonlinear trends produced by the SST and Spalart-Allmaras techniques. Several functional relationships were examined to curve fit the computed points, including cubic and higher order polynomials. However, the best fitting equation was found to use the sine function and took the form

$$E_x = A + B \sin(C y^+ + D) \quad (13)$$

where E_x is the error in drag coefficient at station x and A, B, C, D are the curve fitting coefficients. Although it was desired to fit each curve over the entire range of data, it was only possible to do so for the SST results without compromising the quality of the fit for y^+ values nearer to the wall. This is why Figure 8 has no curve above $y^+ = 10$.

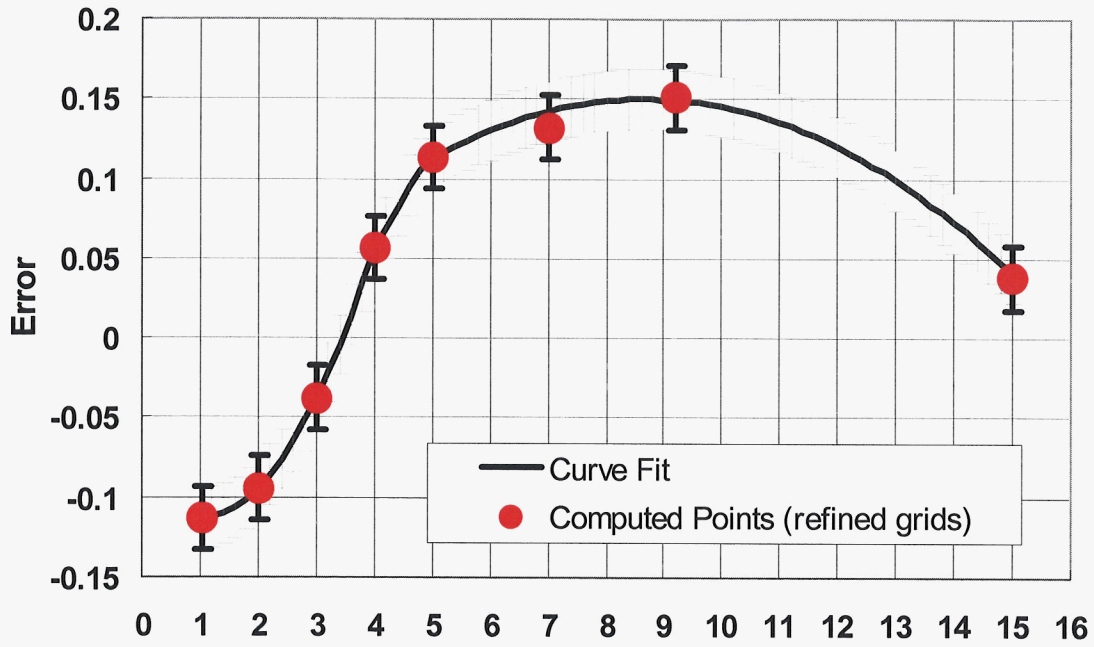


Figure 7. Error Versus Initial Point Spacing for the Menter SST Turbulence Model

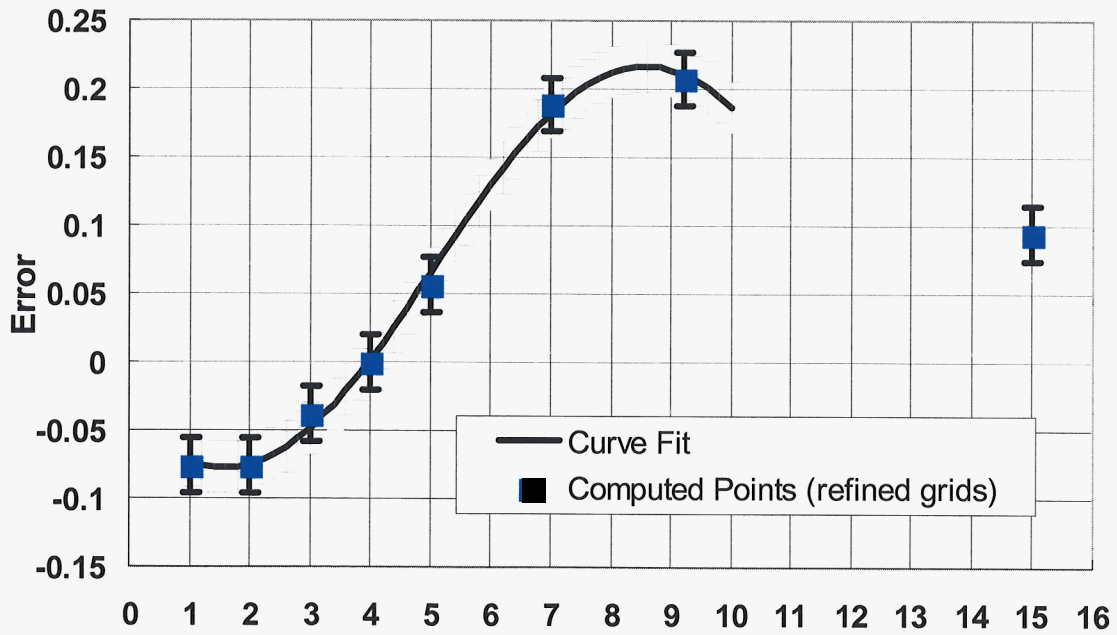


Figure 8. Error Versus Initial Point Spacing for the Spalart-Allmaras Model

Since the flow velocity was only known to two significant figures, there was an inherent uncertainty in the second digit of the computed drag coefficients. To account for this a band of uncertainty was centered about the curve fits produced by Equation 13. Its magnitude was chosen to be one significant figure relative to White's value, i.e., $\pm 0.1 \times 10^{-3}$, which equated to bounding bars of ± 1.89 percent in the figures. This value is commensurate with the aforementioned numerical error of 2 percent which is visualized via error bars of ± 2 percent about each computed point.

The close fits produced by Equation 13 reveal that when the initial cell lies entirely within the laminar sublayer, where $y^+ \leq 5$, the magnitude of the drag error is contained within 12 percent for the SST turbulence model and within 8 percent for the Spalart-Allmaras method. Figure 7 also discloses: (1) a nearly symmetric behavior of the SST errors about zero when $2 \leq y^+ \leq 5$, and (2) a further change in error between $y^+ = 2$ and 1. In contrast to these observations, Figure 8 indicates the Spalart-Allmaras error to be: (1) more sinusoidal in the sublayer, and (2) constant between $y^+ = 2$ and 1.

Outside the sublayer, the error is seen to peak between $y^+ = 8$ and 9 for both RANS techniques, followed by a steady decrease—but this trend is deceiving. As Figures 3 and 4 show, the velocity profiles are not accurate for cells larger than the sublayer. Moreover, Figures 5 and 6 demonstrate the flattening trend that occurs with the skin friction curves as y^+ increases. Since the total drag is determined by integrating the area under each such curve, it is the flattening trend that causes the apparent decrease in error. In short, when grid cells are larger than the laminar sublayer the skin friction errors will yield deceiving values for total drag. For this reason, the aerodynamic designer must insure that $y^+ \leq 5$ for cells adjacent to the wall, at least for very low speed, incompressible cases like the plate studied herein. However, with increasing Reynolds number the requirement may become more severe. Nevertheless, for the plate under consideration, the designer could employ y^+ up to 5 if the associated error in drag coefficient can be tolerated.

B. The Nichols-Nelson Hybrid (RANS/LES) SST Model

With regards to the Nichols-Nelson Hybrid SST Model, it was found that the spatial resolution of the computational domain made a significant difference in the drag coefficients it produced. For example, when y^+ was set to 3 and the grid construction guidelines employed, the solution grid yielded a drag coefficient of 5.2×10^{-3} —a value that corresponded well with the value of 5.1×10^{-3} produced by both the SST and Spalart-Allmaras methods. However, when the spatial grid density was increased by a factor of 10, the drag coefficient decreased drastically to 3.1×10^{-3} . As previously mentioned, this was due to finer turbulence scales being resolved by the more refined grid such that the SST constituent of the model was not operating on a very large part of the flowfield. This fact is demonstrated by comparing contours of the turbulence to grid scale ratios, L_T/L_G , in Figures 9 and 10 which display regions where the ratio is greater than 2. Correspondingly, when the ratio was less than 2 for a large part of the field—presented as unfettered white space—the computed drag coefficients were very similar to those of the RANS techniques as shown in Table 4. Thus, it was established that the Nichols-Nelson Hybrid model

can be applied to steady flows even though it was formulated for unsteady conditions. This attribute might have been anticipated since the model is intended to operate like a RANS method when the turbulence scales are not adequately resolved.

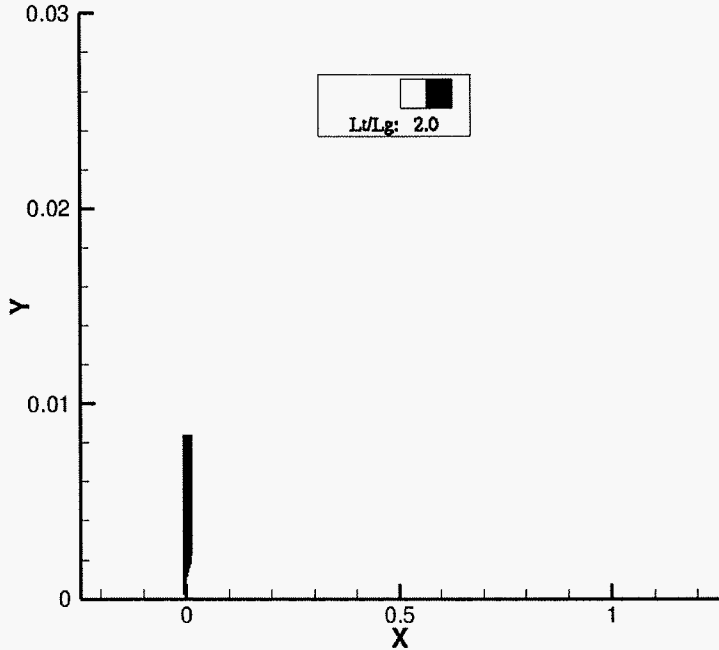


Figure 9. Contours of L_T/L_G for $y^+ = 3$ —Guideline Grid

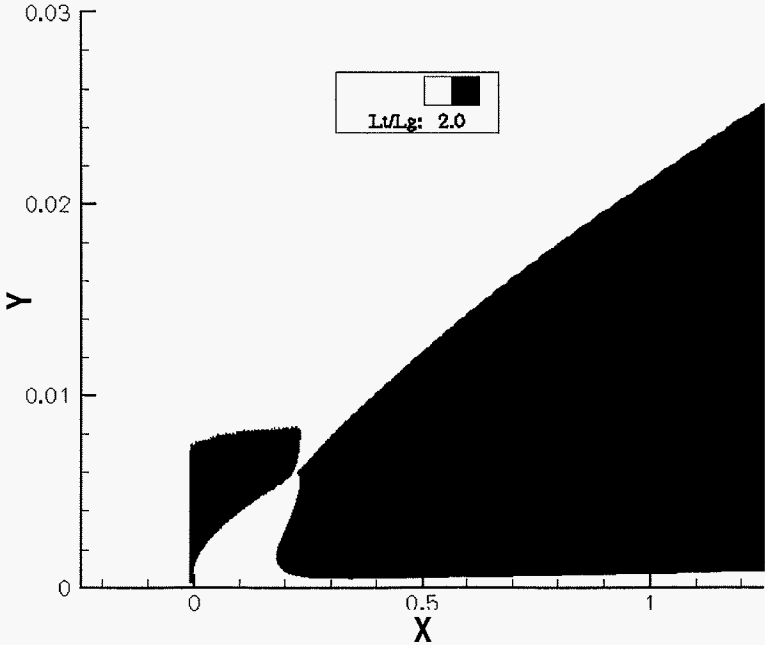


Figure 10. Contours of L_T/L_G for $y^+ = 3$ —Highly Refined Grid

Table 4. Comparison of Drag Coefficients from the Menter SST, Spalart-Allmaras, and Nichols-Nelson Hybrid (RANS/LES) SST Turbulence Models for $L_T/L_G < 2$ Throughout Most of the Flowfield—RANS Results Reported for the Most Refined Grids

y^+	C_D (SST)	C_D (Spalart-Allmaras)	C_D (Nichols-Nelson)
1	4.7×10^{-3}	4.9×10^{-3}	4.5×10^{-3}
2	4.8×10^{-3}	4.9×10^{-3}	4.8×10^{-3}
3	5.1×10^{-3}	5.1×10^{-3}	5.2×10^{-3}
4	5.6×10^{-3}	5.3×10^{-3}	5.7×10^{-3}
5	5.9×10^{-3}	5.6×10^{-3}	6.0×10^{-3}
7	6.0×10^{-3}	6.3×10^{-3}	6.2×10^{-3}
9	6.1×10^{-3}	6.4×10^{-3}	6.2×10^{-3}
15	5.5×10^{-3}	5.7×10^{-3}	5.5×10^{-3}

Profiles of the non-dimensional streamwise velocity are displayed in Figure 11 for solutions resulting from the gridding guidelines. By comparing it with Figures 3 and 4, one can observe that RANS-like behavior and analogous comparisons with Guo’s Self-Similarity Law are exhibited by all but the $y^+ = 1$ curve. This plot deviates very noticeably from all the other results above $y^+ = 10$. Upon examination of the L_T/L_G contours, it was found that this ratio was less than 2 for most of each flowfield until $y^+ = 1$ was reached. For that field, the ratio exceeded 2 for the outer part of the boundary layer from $x = 0.3 L$ onwards—consistent with the previous findings.

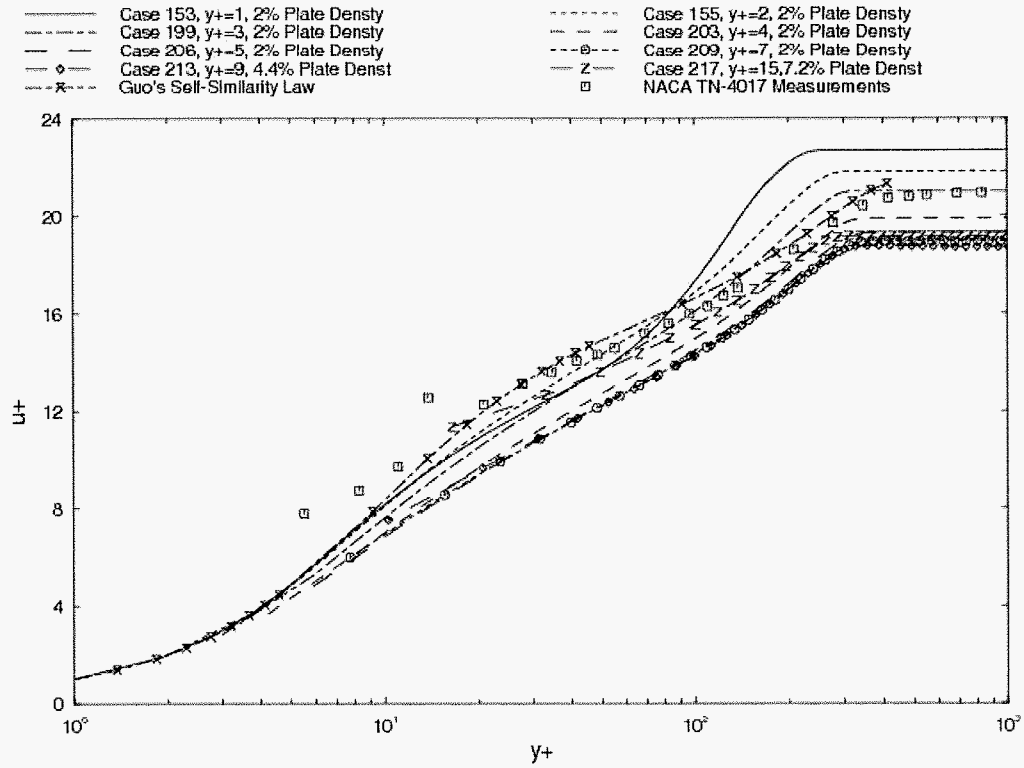


Figure 11. Profiles of u^+ for the Nichols-Nelson Hybrid SST Turbulence Model at $x/L=0.9308$ —Guideline Grids

The corresponding skin friction graph is shown in Figure 12. Comparing it with the Menter SST results in Figure 5, the striking similarities can be detected. It is only by close scrutiny of the middle part of Figure 12 that the solid line of the $y^+ = 1$ result can be discerned just below all the other curves.

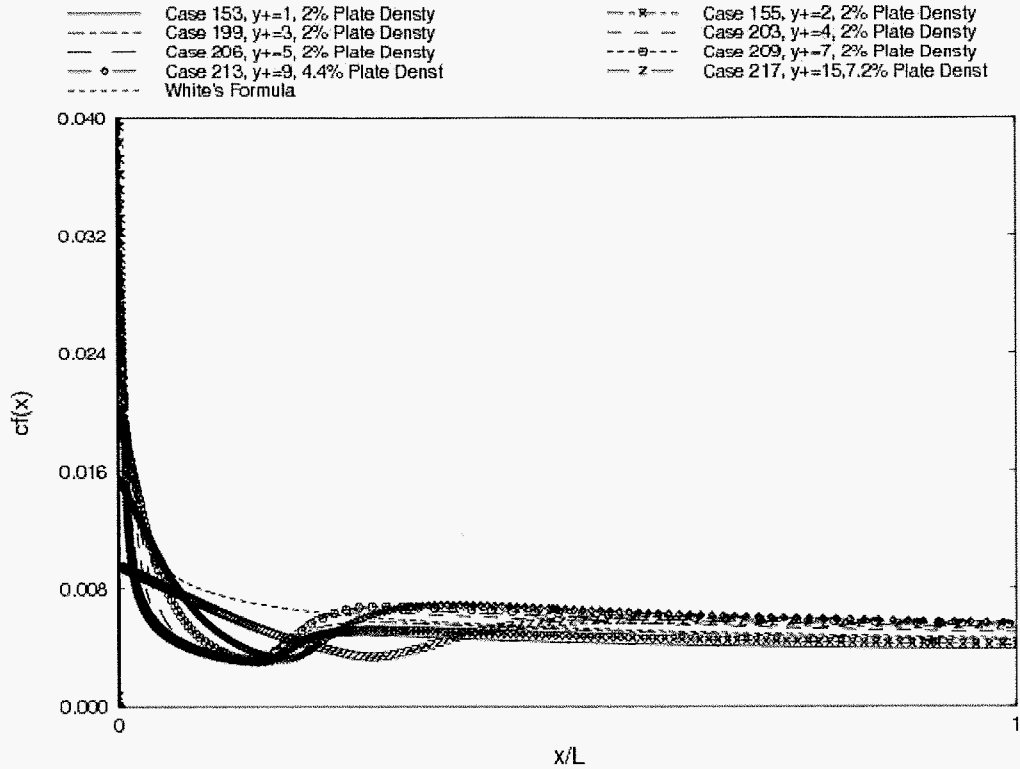


Figure 12. Local Skin Friction Coefficient, $c_f(x)$, for the Nichols-Nelson Hybrid SST Model—Guideline Grids

Results for the error in drag coefficient are found in Figure 13. As before, Equation 13 was exercised to fit the computed data while invoking the same uncertainty and error bars of ± 1.89 percent and ± 2 percent, respectively. The data could only be fit to $y^+ = 5$ without compromising its fidelity to the near-wall computed values. As would be expected after the previous observations, the correlation of drag error with initial spacing is similar to those of Figures 7 and 8. Likewise, it is evident that the aerodynamic designer must ensure that surface grid cells are completely contained within the laminar sublayer to avoid deceptive drag values.

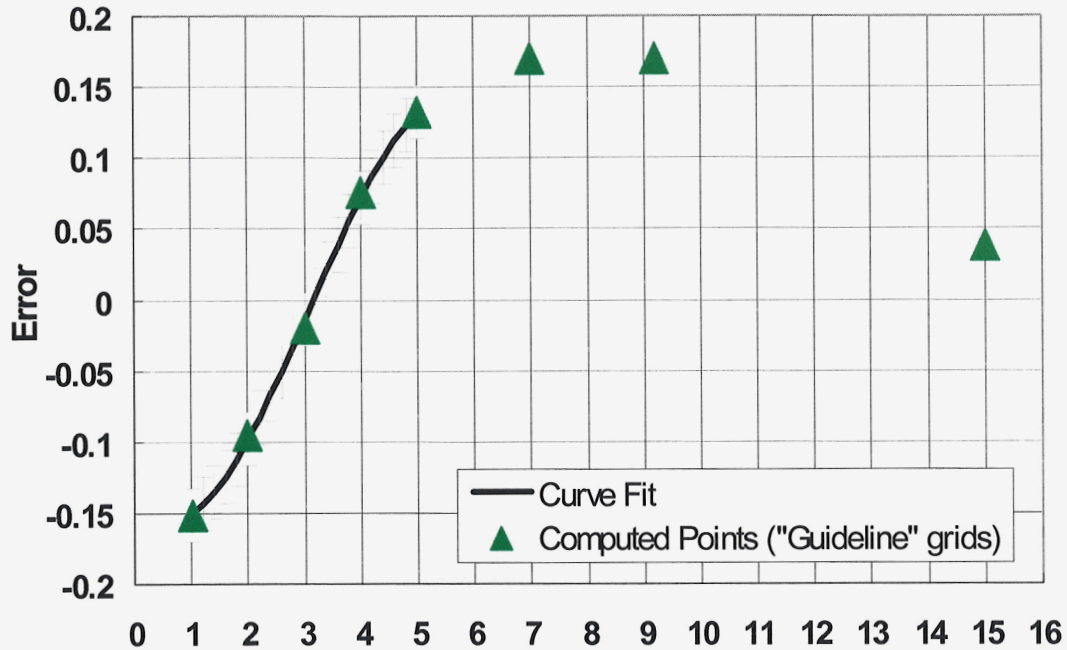


Figure 13. Error Versus Initial Point Spacing for Nichols-Nelson Hybrid SST Model

IV. SUMMARY

It has been shown that the error in drag coefficient for a unit flat plate within an incompressible flowfield correlates with initial grid point spacing for the Menter Shear Stress Transport (SST) and Spalart-Allmaras RANS turbulence models as well as for the Nichols-Nelson Hybrid (RANS/LES) SST turbulence model. The correlations for each model are nonlinear relationships that can be represented in terms of the sine function. Uncertainty in the flow velocity was ± 1.89 percent which was commensurate with the numerical error of ± 2 percent in each computation. Further, it was learned that when the turbulence to grid length scale ratio is less than two for most of the turbulent field, the Nichols-Nelson Hybrid SST model produces RANS-like values. Thus, this unsteady model was found to be applicable to steady-state flows, provided the grid was not too refined. These results in concert with examinations of the skin friction and non-dimensional streamwise velocity profiles made it clear that grid cells adjacent to the wall must be completely contained within the laminar sublayer, where $y^+ \leq 5$, to obtain meaningful results.

REFERENCES

1. Shivananda, T. P, Zabrensky, E. F., McKeel, S. A., and Papay, M. L., "Comparison of Engineering and CFD Predictions and Wind Tunnel Data for a Launch Vehicle Configuration," AIAA Paper 1997-2251.
2. Dillenius, M. F. E., Lesieutre, D. J, Hegedus, M. C., Perkins, S. C. Jr., Love, J. F., and Lesieutre, T. O., "Engineering, Intermediate, and High Level Aerodynamic Prediction Methods and Applications," AIAA Paper 1997-2278.
3. Srivastava, B., "CFD Analysis and Validation of Lateral Jet Control of a Missile," AIAA Paper 96-0288.
4. Raj, P., "Requirements for Effective Use of CFD in Aerospace Design," Surface Modeling, Grid Generation and Related Issues in Computational Fluid Dynamics (CFD) Solutions, NASA Conference Publication 3291, 1995, pp.15-28.
5. Srivastava, B., Furtek, J., Shelton, A., Paduano, R., "Role of CFD in Missile Aerodynamic Design: A Review of Recent Efforts at Raytheon," NATO/RTO Symposium of the Applied Vehicle Technology Panel of Missile Aerodynamics, Sorento, Italy, 1998, pp. 33-1 – 33-19.
6. Brédif, M., Chapin, F., Borel, C., and Simon, P., "Industrial Use of CFD for Missile Studies: New Trends at MATRA BAe DYNAMICS France," NATO/RTO Symposium of the Applied Vehicle Technology Panel of Missile Aerodynamics, Sorento, Italy, 1998, pp 32-1 – 32-14.
7. Vaughn, M.E., Jr. and Auman, L. M., "A Productivity-Oriented Application of Computational Fluid Dynamics to the Design of a Hypervelocity Missile," AIAA Paper 2002-2937.
8. Vaughn, M. E., Jr., "Guidelines for Gridding Incompressible, Laminar, Flat Plate Flows," AIAA Paper 2004-2231.
9. Menter, F. R., "Zonal Two Equation $k-\omega$ Turbulence Models for Aerodynamic Flows," AIAA Paper 1993-2906.
10. Spalart P. R. and Allmaras, S. R., "A One-Equation Turbulence Model for Aerodynamic Flows," AIAA Paper 1992-0439.
11. Nichols, R. H. and Nelson, C. C., "Application of Hybrid RANS/LES Turbulence Models," AIAA Paper 2003-0083.
12. Spalart, P., Jou, W.-H., Strelets, M., and Allmaras, S., "Comments on the Feasibility of LES for Wings and on a Hybrid RANS/LES Approach," Eds. C. Liu and Z. Liu, Greyden Press, Columbia, OH, August 1997.

REFERENCES (CONTINUED)

13. Vaughn, M. E., Jr., Gridding Guidelines for Numerical Solutions of Simple Flows, Ph.D. thesis, Department of Mechanical Engineering, University of Alabama in Huntsville, Huntsville, AL, published November 2007.
14. Mickley, H. S. and Davis, R. S., "Momentum Transfer for Flow Over a Flat Plate with Blowing," NACA TN 4017, 1957.
15. ¹⁵ Nichols, R. H., "Comparison of Hybrid Turbulence Models for a Circular Cylinder and a Cavity," AIAA Journal, Vol. 44, No 6, pp. 1207-1219, June 2006.
16. Schlichting, H., Boundary-Layer Theory, 6th ed., McGraw-Hill, New York, 1968.
17. White, F. M., Viscous Fluid Flow, 3rd ed., McGraw-Hill, New York, 2006.
18. Guo, J, "Self-Similarity of Mean-Flow in Pipe Turbulence," AIAA Paper 2006-2885.
19. Coles, D. E., "The Young Person's Guide to the Data," Proceedings Computation of Turbulent Boundary Layers—1968 AFOSR-IFP-Stanford Conference, Volume II Compiled Data, edited by D. E. Coles and E. A. Hirst, Department of Mechanical Engineering, Stanford University, CA, 1969, pp. 1-45.
20. Roache, P. J., Verification and Validation in Computational Science and Engineering, Hermosa, Albuquerque, New Mexico, 1998, Chapter 5, pp. 112-115, 129-130.
21. Nelson, C. C. and Roy, C. J., "Verification of the Wind-US CFD Code Using the Method of Manufactured Solutions," AIAA Paper 2004-1104.
22. Wilcox, D. C., Turbulence Modeling for CFD, 2nd ed., DCW Industries, La Cañada, CA, 1998, Section 4.9.2, pp. 193-197.

INITIAL DISTRIBUTION LIST

		<u>Copies</u>
Weapon Systems Technology Information Analysis Center 1901 N. Beauregard Street, Suite 400 Alexandria, VA 22311-1720	Mr. Perry Onderdonk ponderdonk@alionscience.com	Electronic
Defense Technical Information Center 8725 John J. Kingman Rd., Suite 0944 Fort Belvoir, VA 22060-6218	Jack Rike jrike@dtic.mil	Electronic
AMSRD-AMR		Electronic
AMSRD-AMR-CS-IC		Electronic
AMSRD-AMR-SS,	Mr. Gregory B. Tackett Gregory.Tackett@us.army.mil	Electronic
AMSRD-AMR-SS-AT,	Mr. Lamar M. Auman lamar.auman@us.army.mil Mr. Milton E. Vaughn, Jr. Ed.Vaughn@us.army.mil	Electronic Electronic
AMSRD-L-G-I,	Ms. Anne Lanteigne anne.lanteigne@us.army.mil	Electronic